Published OnlineFirst February 7, 2018; DOI: 10.1158/1535-7163.MCT-17-0965

Models and Technologies

Molecular Cancer Therapeutics

Characterizing the Potency and Impact of Carbon Ion Therapy in a Primary Mouse Model of Soft Tissue Sarcoma

Jeremy M. Brownstein[1], Amy J. Wisdom[2], Katherine D. Castle[2], Yvonne M. Mowery[1], Peter Guida[3], Chang-Lung Lee[1], Francesco Tommasino[5,6], Chiara La Tessa[4,5,6], Emanuele Scifoni[5], Junheng Gao[7], Lixia Luo[1], Lorraine Da Silva Campos[1], Yan Ma[1], Nerissa Williams[1], Sin-Ho Jung[7], Marco Durante[5], and David G. Kirsch[1,2]

Abstract

Carbon ion therapy (CIT) offers several potential advantages for treating cancers compared with X-ray and proton radiotherapy, including increased biological efficacy and more conformal dosimetry. However, CIT potency has not been characterized in primary tumor animal models. Here, we calculate the relative biological effectiveness (RBE) of carbon ions compared with X-rays in an autochthonous mouse model of soft tissue sarcoma. We used Cre/loxP technology to generate primary sarcomas in $Kras^{LSL\text{-}G12D/+}$; $p53^{fl/fl}$ mice. Primary tumors were irradiated with a single fraction of carbon ions (10 Gy), X-rays (20 Gy, 25 Gy, or 30 Gy), or observed as controls. The RBE was calculated by determining the dose of X-rays that resulted in similar time to posttreatment tumor volume quintupling and exponential growth rate as 10 Gy carbon ions. The median tumor volume quintupling time and exponential growth rate of sarcomas treated with 10 Gy carbon ions and 30 Gy X-rays were similar: 27.3 and 28.1 days and 0.060 and 0.059 mm^3/day, respectively. Tumors treated with lower doses of X-rays had faster regrowth. Thus, the RBE of carbon ions in this primary tumor model is 3. When isoeffective treatments of carbon ions and X-rays were compared, we observed significant differences in tumor growth kinetics, proliferative indices, and immune infiltrates. We found that carbon ions were three times as potent as X-rays in this aggressive tumor model and identified unanticipated differences in radiation response that may have clinical implications. *Mol Cancer Ther; 17(4); 858–68. ©2018 AACR.*

Introduction

Nearly four in ten Americans will develop cancer during their lifetimes, and approximately half of those afflicted will undergo radiation therapy (1). Currently, most radiation treatments are delivered using linear accelerators to generate and collimate high-energy X-ray photons (2). Charged particle radiation, which is created by accelerating protons, carbon ions, or other atomic nuclei, can have a dosimetric advantage over X-ray based treatments (3). Because X-rays enter the patient in front of the target and then exit the patient behind the target, multiple X-ray fields that overlap within the target volume are often required to safely deliver an adequate dose to the tumor, which can expose large volumes of normal tissue to low doses of radiation (4). Unlike photons, charged particles traversing matter slow down and eventually halt, releasing a narrow burst of energy, known as a Bragg Peak, just prior to stopping (3). Because minimal energy is deposited beyond the Bragg Peak, charged particle radiation deposits a much lower dose distal to the target, resulting in a smaller volume of nontarget tissue exposed to radiation (5). Thus, proton radiotherapy may have advantages over photons in the treatment of some pediatric brain tumors and other tumor types where minimizing low-dose exposure to adjacent tissues is critical (6). Carbon ions have similar dosimetric advantages as protons, but they are more biologically potent than either protons or photons (7). There is thus growing interest in carbon ion therapy (CIT) in the treatment of biologically aggressive cancers (8, 9).

Within the Bragg peak, heavy ions such as carbon have a high linear energy transfer (LET) because they deposit more energy (keV) per unit distance (μm) than low LET protons and photons (7). Carbon ions create denser ionization tracks, which cause more clustered DNA damage. Such damage is often irreparable and more likely to result in mitotic cell death, even in otherwise radioresistant cells (10). When photons and protons damage DNA, molecular oxygen (if present) significantly potentiates cell kill by reacting with damaged loci, making DNA breaks difficult to repair. Because carbon ions create complex genetic injuries even in the absence of oxygen, hypoxic tumors are comparatively less resistant (11). Additionally, *in vitro* data and experiments with transplanted tumor models suggest that carbon ions better activate the immune system (12) and decrease tumor metastatic potential (13). Therefore, CIT may treat cancer more effectively and consistently than treatment with either photons or protons.

[1]Department of Radiation Oncology, Duke University Health System, Durham, North Carolina. [2]Department of Pharmacology & Cancer Biology, Duke University, Durham, North Carolina. [3]Department of Biology, Brookhaven National Laboratory, Upton, New York. [4]Brookhaven National Laboratory, Upton, New York. [5]Trento Institute for Fundamental Physics and Applications, National Institute for Nuclear Physics (INFN), Trento, Italy. [6]Department of Physics, University of Trento, Trento, Italy. [7]Department of Biostatistics and Informatics, Duke University, Durham, North Carolina.

Note: Supplementary data for this article are available at Molecular Cancer Therapeutics Online (http://mct.aacrjournals.org/).

Corresponding Author: David G. Kirsch, Duke University, 450 Research Drive, Durham, NC 27708. Phone: 919-681-8586; Fax: 919-668-7345; E-mail: david.kirsch@duke.edu

doi: 10.1158/1535-7163.MCT-17-0965

Published OnlineFirst February 7, 2018; DOI: 10.1158/1535-7163.MCT-17-0965

The relative biological effectiveness (RBE) is a ratio that quantifies the relative efficiency with which radiation of two different qualities causes a specific effect, such as tissue damage or tumor growth delay. For example, the RBE of CIT can be calculated by dividing the dose of 250 keV X-rays by the particle's isoeffective dose, which is the quantity of particle radiation required to cause the same biological effect as the X-ray treatment (13). Under clinical conditions, the RBE of carbon in normal tissues and tumor cells can vary but generally ranges between 2 and 3 (10, 14–17), with some studies demonstrating lower or higher values. Many factors impact RBE including the physical characteristics of the radiation (i.e., LET, fraction size; refs. 18, 19) and the biological characteristics of the treated volume (i.e., intrinsic radiosensitivity, tissue oxygen tension; refs. 8, 14, 20).

Carbon ions have an energy-dependent range and only deposit high LET radiation within their narrow Bragg peak (7). Therefore, covering the full breadth of a target requires a poly-energetic beam, which produces many Bragg peaks that sum to form a spread-out Bragg peak (SOBP; ref. 10). The requisite spectrum of energies can be attained from a monoenergetic beam by attenuating it through an oscillating/rotating variable-depth compensator using a technique known as passive spreading. Alternatively, active scanning systems can "paint" dose onto each successive layer of the target by incrementally modulating the primary beam energy. These delivery techniques are currently employed to treat human cancers at a few CIT facilities throughout Europe and Asia (7).

The UC Lawrence Berkeley Research Laboratory pioneered the use of charged ion radiotherapy, utilizing protons and helium ions in the 1950s to treat pituitary adenomas and subsequently incorporating heavier ions in the 1970s (8). Since the closure of this hadron research program in 1993, the clinical use of carbon ion radiotherapy is now only employed outside the United States (9). Although results from two ongoing randomized controlled trials comparing CIT with other forms of radiation therapy are not available, a recent review of the outcomes of patients treated with CIT in Chiba, Japan compared favorably with historical controls. For example, historical data show the two-year survival rate for locally advanced pancreatic adenocarcinoma is 20% for patients treated with definitive X-ray chemoradiation (21), but a retrospective series of 47 patients treated with CIT in Chiba, Japan showed a 2-year survival rate of 48% (22). In another retrospective series, 51% of patients with recurrent rectal cancer treated with carbon ions remained alive at 5 years, surpassing the 25% 5-year survival observed in patients treated with X-ray radiation (23). Although these nonrandomized retrospective comparisons should be interpreted with caution, the encouraging treatment outcomes of CIT in certain radioresistant tumors certainly warrant further investigation.

Much of our understanding of how carbon ions affect human cancer is based on extrapolation from their impact on tumor cell lines and transplanted tumor models (20, 24–29). Although informative, these systems often lack the heterogeneity of human malignancies and poorly approximate a natural stromal/immune response. Thus, to better investigate the impact of CIT on naturally occurring malignant tumors, we explored its effects in a radioresistant autochthonous mouse model of soft tissue sarcoma (30). Tumor-bearing mice were treated with either CIT or X-ray radiotherapy, and treatment efficacy was quantified by measuring tumor growth delay. We demonstrate that the RBE of carbon ions in this primary genetically engineered mouse model of sarcoma is approximately 3, and we observe differences in both tumor response and recurrence following CIT.

Materials and Methods

Mouse experiments

The goal of this study was to quantify the RBE of carbon ion radiotherapy relative to X-ray radiotherapy in an autochthonous genetically engineered mouse model of soft tissue sarcoma (31). Sarcomas in tumor-bearing mice ranging in size from 40 to 120 mm^3 were treated with either a single fraction of 10 Gy carbon ion radiation therapy or 20, 25, or 30 Gy X-rays. After treatment, tumor volumes were tracked with serial caliper measurements three times weekly. The experimental schema is outlined in Fig. 1A.

Tumor model

All animal studies were approved by the IACUC from both Duke and Brookhaven National Laboratory (BNL). Mixed-background, mixed-gender $Kras^{LSL\text{-}G12D};p53^{fL/fL}$ (KP) mice with conditional mutations in oncogenic K-ras and both alleles of p53 (Fig. 1B) were injected into the gastrocnemius muscle with an adenovirus expressing Cre recombinase as previously described (31). At the time of injection, mice were 6 to 12 weeks old (median 8 weeks). At 8 to 12 weeks after injection, mice developed sarcomas that share histological and gene expression features with human undifferentiated pleomorphic sarcoma (32).

Radiation techniques

Carbon ion radiation therapy was delivered at the NASA Space Radiation Laboratory at BNL, Upton NY. A 109.5 MeV/nucleon beam was modulated through a spinning 30-spoke custom 3D-printed acrylonitrile butadiene styrene compensator wheel (0.97 g/cc). Spoke thickness varied incrementally between 0 and 2.9 cm. Spoke arc lengths were optimized to yield a 3 cm SOBP with a constant physical dose delivered throughout the treatment volume. The carbon ion beam was shaped by a copper collimator, yielding a circular treatment field with a 15 mm diameter (Fig. 1C and D).

At the beginning of each treatment day, quality assurance testing included dose rate measurements and verification that the peak-to-plateau ratio throughout the SOBP was consistent with predictions. Prior to irradiation, mice were anesthetized with intraperitoneal ketamine/xylazine (80/8 mg/kg) and were immobilized with their sarcomas centered in the collimator portal. The single fraction 10 Gy treatment was administered at a dose rate of 2.4 Gy/minute.

X-ray radiation therapy was delivered at Duke University, Durham, NC. The X-RAD 225Cx small animal irradiator (precision X-ray) was utilized for image-guided radiotherapy (33). The treatment beam employed 13 mA 225 kV X-rays attenuated through a 0.3 mm copper treatment filter; imaging employed 2.5 mA 40 kV X-rays. The X-ray beam was shaped by a copper collimator, yielding a 40 × 40 mm square field at isocenter. Prior to irradiation, mice were anesthetized with isoflurane and immobilized on the treatment stage with continuous isoflurane administered via nose cone. To assess for interaction between radiation and anesthesia, a cohort of tumor-bearing mice allocated to 20 Gy X-rays was anesthetized with ketamine/xylazine (as above) and was compared to similarly treated mice anesthetized with isoflurane. The isocenter was aligned

Published OnlineFirst February 7, 2018; DOI: 10.1158/1535-7163.MCT-17-0965

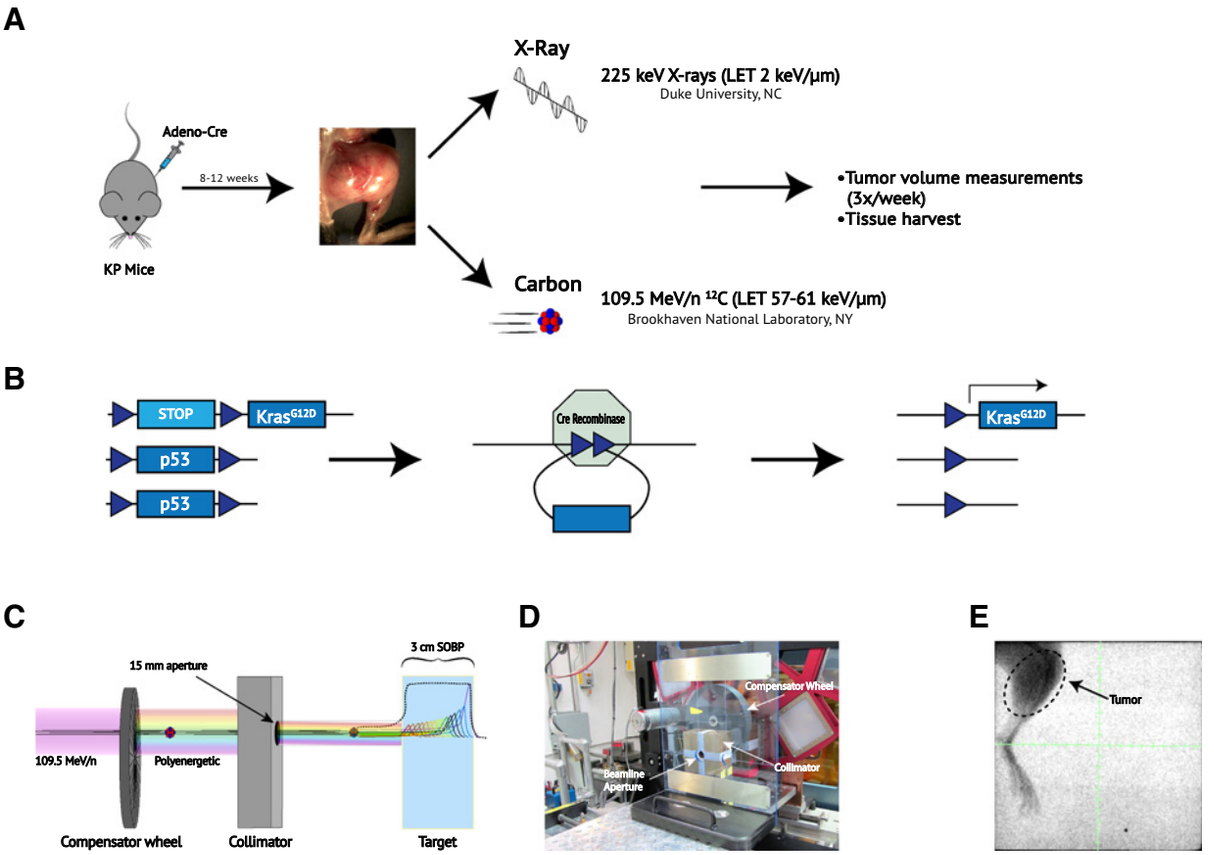

Figure 1.

Schematic of the experimental design and radiation therapy treatments. **A,** Schematic of the experimental design. Mice with conditional mutations in oncogenic Kras and p53 (*Kras*$^{LSL\text{-}G12D}$;*p53*$^{fl/fl}$ or KP) were inoculated with adenovirus expressing Cre recombinase via direct injection into muscle of the hind-limb, thus generating primary sarcomas. Mice were either treated with X-rays at Duke or were transported to BNL for CIT (**B**) Cre recombinase recombines LoxP sites (blue triangles) in *Kras*$^{LSL\text{-}G12D}$; *p53*$^{fl/fl}$ (KP) mice, selectively deleting p53 and activating the expression of mutant Kras by deleting the transcription stop cassette. **C,** Schematic of carbon ion radiation delivery. A mono-energetic carbon ion beam passes through a spinning variable-depth compensator wheel and is shaped by a copper collimator. The resulting poly-energetic beam produces many Bragg peaks that span the breadth of the target (colored lines) and effectively sum to create a spread-out Bragg peak (SOBP) (black line). **D,** Carbon ion experimental setup at NSRL. The compensator wheel and collimator are arranged within the beamline. **E,** Image-guided X-ray radiotherapy. Pre-treatment fluoroscopic imaging depicts a 40 × 40 mm square field encompassing the sarcoma-bearing leg and excludes the remainder of the mouse. Tick marks = 2 mm.

under fluoroscopic image guidance. Radiotherapy was delivered with equally weighted AP/PA fields which encompassed the tumor-bearing leg while sparing the remainder of the mouse (Fig. 1E). A single fraction of either 20, 25, or 30 Gy was administered at a dose rate of 3 Gy/minute.

To assess for the potential impact of differences in handling and environment between BNL and Duke University Medical Center, littermates of mice treated at both locations were followed as untreated controls. Serial tumor measurements were collected from untreated controls once their sarcomas met size eligibility for treatment (40–120 mm^3).

Histologic analysis

All immunohistochemistry, immunofluorescence, and hematoxylin and eosin staining was performed on paraffin-embedded tumor sections (30). Tissue specimens were fixed in 10% neutralized formalin for 24 to 48 hours and preserved in 70% ethanol until paraffin embedding. Four micron sections were de-waxed with xylene and rehydrated with a graded series of ethanol and water washes prior to staining. For Ki-67 immunohistochemistry, the primary antibody utilized was mouse anti-Ki-67 IgG (1:200, BD Pharmingen, #550609), and the secondary antibody utilized was biotinylated horse anti-mouse IgG (1:200, Vector Laboratories, #BA-2000). For phospho-histone H3 immunofluorescence, the primary antibody utilized was rabbit polyclonal antibody to H3 (phospho S10; 1:200, Abcam, #ab5176), and the secondary antibody utilized was Alexa Fluor 555 goat anti-rabbit IgG (1:200; Invitrogen, #A-21429). Nuclear staining was performed using DAPI (Thermo Fisher Scientific, #P36962). For CD3 staining, the primary antibody was rabbit monoclonal IgG antibody to CD3 (1:100; Thermo Fisher Scientific, #9107-S) and the secondary antibody was polymer-HRP anti-rabbit DAKO Envision+ kit as per manufacturer instructions (Agilent, #K4011). TUNEL staining was performed with the Click-IT Plus TUNEL Assay Alexa Fluor 594 as per manufacturer's instructions (Thermo Fisher Scientific). Pictures were acquired with a Leica DFC340 FX fluorescence

Published OnlineFirst February 7, 2018; DOI: 10.1158/1535-7163.MCT-17-0965

microscope (Leica Microsystems) with a 200× objective using Leica Suite software (Leica Microsystems). Quantification was performed using ImageJ (NIH).

Dose distribution/LET calculations

The dose distribution and dose-weighted LET densities were calculated utilizing Monte Carlo simulations based on the Hadrontherapy Code included in Geant4 (34). Specifically, the wheel modulation was simulated according to a recent extension of the code (35). We assumed a 15 mm circular beam with a 109.5 MeV/n beam energy (0.5 MeV/n initial energy spread) and scored the physical dose and LET in a homogenous water-density target. Dose calculations were obtained by using 0.1 mm edge length cubic voxels and integrating over a central 10 mm corridor in the water phantom. Because of the long computational time, the information on LET along the SOBP was obtained with a voxel size of 0.5 mm, integrating over a single-voxel central corridor.

Measurements and statistics

A caliper was used to measure bi-dimensional tumor diameter three times per week. Volumes were approximated from bi-dimensional measurements using the following equation (Eq. 1).

$$V = \frac{\pi}{6} \times d_1^2 \times d_2,$$

where V is the volume, d_1 the smaller diameter, and d_2 is the larger diameter. Published *in vitro* and *in vivo* studies have generally reported an RBE for carbon ions between 2 and 3 (10, 14, 16, 17). Therefore, to calculate RBE in the autochthonous sarcoma model, we sought to determine which of the three single doses of X-ray treatments (20, 25, and 30 Gy) induced a similar growth delay as a single fraction of 10 Gy carbon ion radiotherapy. Multiple tests were employed to determine which X-ray dose best approximated the effects of 10 Gy carbon ions. Treatment response was quantified using both time-to-tumor-quintupling and exponential growth rate following radiotherapy. The Mann–Whitney *U* test was used to compare median time-to-tumor quintupling and the exponential growth rate and the Kruskal–Wallis test was used to compare initial volumes between groups.

Histologic data points were calculated by taking the average of either the percent positivity or absolute number of positive cells in six randomly chosen 200× fields per tumor. The Mann–Whitney *U* test was utilized to compare groups (JMP 13, SAS Institute).

Tumor growth model

As expected from a primary mouse tumor model treated with radiation therapy, the sarcomas in this experiment exhibited variable growth patterns following treatment. For example, many tumors initially ceased growing, and only resumed their exponential expansion after a static period of days to months. We thus created a novel piecewise exponential tumor growth model to further characterize subtle differences in growth kinetics following isoeffective treatments. We employed a piecewise linear regression (Eq. 2) to the log-transformation of tumor volume where parameters c and B_1 describe the period of initial growth arrest and the final exponential growth rate, respectively. Parameters were determined using Marquardt iterative methods, and the Mann–Whitney *U* test was utilized to compare parameters between isoeffective groups (SAS 9.4, R 3.2.2).

$$\text{Ln volume} = \begin{bmatrix} B_0 & \text{if } x \le c \\ B_0 + B_1 * (x - c) & \text{if } x > c \end{bmatrix}$$

This piecewise exponential model describes the natural logarithm tumor volume as a function of time. Ln of tumor volume remains at B_0 until time c when it begins to grow linearly with a slope of B_1, where B_0, B_1, and c are parameters of the model.

Results

Treatment delivery

To deliver carbon ions to autochthonous sarcomas in mice, we built a spinning compensator wheel at the NASA Space Radiation Laboratory in BNL to produce a 3 cm constant physical-dose SOBP, comprised of many individual Bragg peaks (Fig. 2A). Measurements were taken on each treatment day, and Monte Carlo simulations confirmed a constant physical dose distribution throughout the tumor volume (Fig. 2B) and a median tumor dose-weighted LET of 59 keV/μm (interquartile range or IQR 57–61 keV/μm; Fig. 2C), which is within the clinically relevant range for CIT (36).

At BNL, 24 primary sarcomas were treated with a single fraction of 10 Gy CIT and 28 untreated sarcomas were followed as untreated controls. At Duke, 44 sarcomas within a comparable size range were treated with X-ray radiotherapy and 10 untreated sarcomas served as untreated controls (Table 1). Initial tumor volume did not differ significantly between treatment groups ($P = 0.10$), and initial tumor volume did not correlate with tumor quintupling time (Pearson $R^2 = 0.01$, $P = 0.43$).

Of the 12 mice treated with 20 Gy X-rays, eight were anesthetized with ketamine/xylazine similar to the carbon ion treated mice, and the remaining four mice were anesthetized with isoflurane. As median quintupling times (MQT) with both anesthetics were similar (MQT 13 days vs. 15 days; $P = 0.76$; Supplementary Fig. S1A), the remaining mice that underwent X-ray treatment were anesthetized with isoflurane. Untreated mice housed at BNL had a MQT of 9.0 days, which was similar to 9.3 days for untreated mice at Duke ($P = 0.67$; Supplementary Fig. S1B). Therefore, we concluded that differences between Duke and BNL did not significantly impact tumor growth. The absolute volume measurements for individual mice in this study are shown in Supplementary Table S1.

Calculating RBE

Following treatment, a dose response relationship was observed in which tumors receiving CIT or higher dose X-rays exhibited slower regrowth than those treated with lower doses of X-ray radiation (Fig. 3A). The MQT for tumors treated with 10 Gy carbon was 27.3 days (range 22–138 days). Tumors treated with 30 Gy X-rays had a similar MQT of 28.1 days (range 21–40 days; $P = 0.93$). However, tumors treated with lower X-ray doses of 25 and 20 Gy quintupled significantly faster: 18.2 days ($P < 0.05$) and 13.5 ($P < 0.001$), respectively (Fig. 3B). An exponential regression of tumor growth following carbon treatment revealed an exponential growth rate of 0.060 mm^3/day, which was similar to 30 Gy X-rays (0.059 mm^3/day; $P = 0.97$). The exponential growth rate was significantly higher for tumors treated with 25 and 20 Gy X-rays (0.099 mm^3/day; $P < 0.05$, and 0.111 mm^3/day; $P < 0.01$, respectively; Fig. 3C). In this mouse model of soft tissue sarcoma,

Published OnlineFirst February 7, 2018; DOI: 10.1158/1535-7163.MCT-17-0965

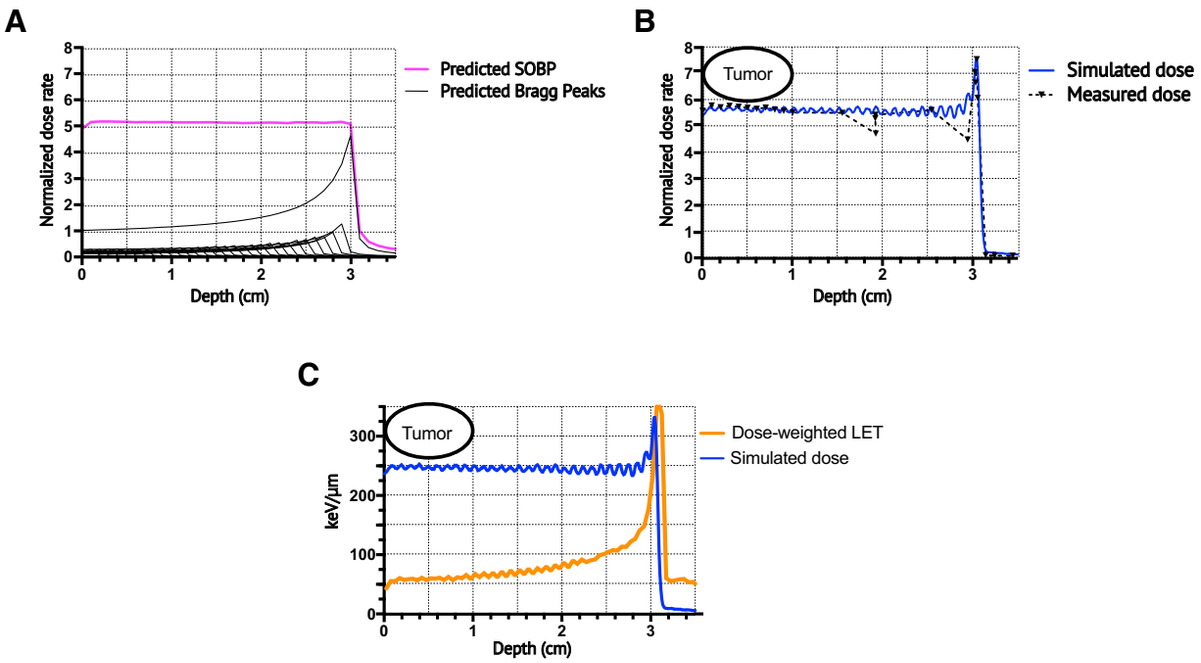

Figure 2.

Carbon ion Spread out Bragg peak (SOBP), predictions, and measurements. **A,** The spinning acrylonitrile butadiene styrene compensator wheel was expected to produce a poly-energetic carbon beam with a 3-cm constant physical dose SOBP (magenta) comprised of 30 individual Bragg peaks (black lines). Dose rate is represented as a function of depth and is normalized to entrance dose rate of mono-energetic 109.5 MeV/nucleon beam = 1. **B,** Monte Carol simulations (blue) and ion chamber dose rate measurements (black-dashed) of the SOBP confirmed a constant physical dose distribution within the target in the proximal SOBP. **C,** Monte Carlo simulated dose-weighted LET (orange) is 59 to 63 keV/µm throughout the proximal SOBP (blue).

treatment with 30 Gy of X-rays was isoeffective to treatment with 10 Gy carbon ions with respect to exponential tumor growth and quintupling time. For these tumor growth endpoints in this primary soft tissue sarcoma model, we thus conclude that the RBE of carbon ions is 3 (Fig. 3D).

Modeling tumor growth kinetics

To determine whether isoeffective treatments had similar patterns of tumor growth delay and regrowth kinetics, we employed a linear regression based on a novel piecewise tumor growth model (Eq. 2; Fig. 4A). We observed that this piecewise approach better characterized the dynamics of KP tumor growth following radiation treatment than did a simple exponential model (Fig. 4B). Figure 4C and D demonstrate the piecewise growth model applied to individual mice treated with carbon ions and X-rays, respectively. Sarcomas treated with 10 Gy carbon had an estimated median growth delay of 13.5 days (IQR 12–20 days), which was not significantly longer than 12.1 days (IQR 8–17 days) in

Table 1. Number of tumor-bearing KP mice assigned to each experimental group

BNL, Upton, NY		Duke University, Durham, NC	
Untreated controls[a]	28	Untreated controls[a]	10
Received 10 Gy CIT[b,c]	24	Received 20 Gy X-rays[a]	12
● Followed for growth delay[a]	16	● Anesthetized with ketamine[b,d]	8
● Harvested for tissue analysis[e]	7	● Anesthetized with isoflurane[f]	4
○ 4 hours posttreatment	1	Received 25 Gy X-rays[a,f]	8
○ 24 hours posttreatment	3	Received 30 Gy X-rays[f]	17
○ 48 hours posttreatment	3	● Followed for growth delay[a]	8
		● Harvested for tissue analysis[e]	9
		○ 24 hours posttreatment	4
		○ 48 hours posttreatment	5
Total	52	Total	47

[a]Followed for growth delay.
[b]Anesthetized with intraperitoneal ketamine and xylazine.
[c]One mouse moved out of treatment portal during CIT and was thus omitted from all analyses.
[d]Two mice treated with 20 Gy X-rays succumbed prior to tumor quintupling and were thus omitted from the quintupling time analysis.
[e]Harvested for tissue analysis.
[f]Anesthetized with isoflurane.

Published OnlineFirst February 7, 2018; DOI: 10.1158/1535-7163.MCT-17-0965

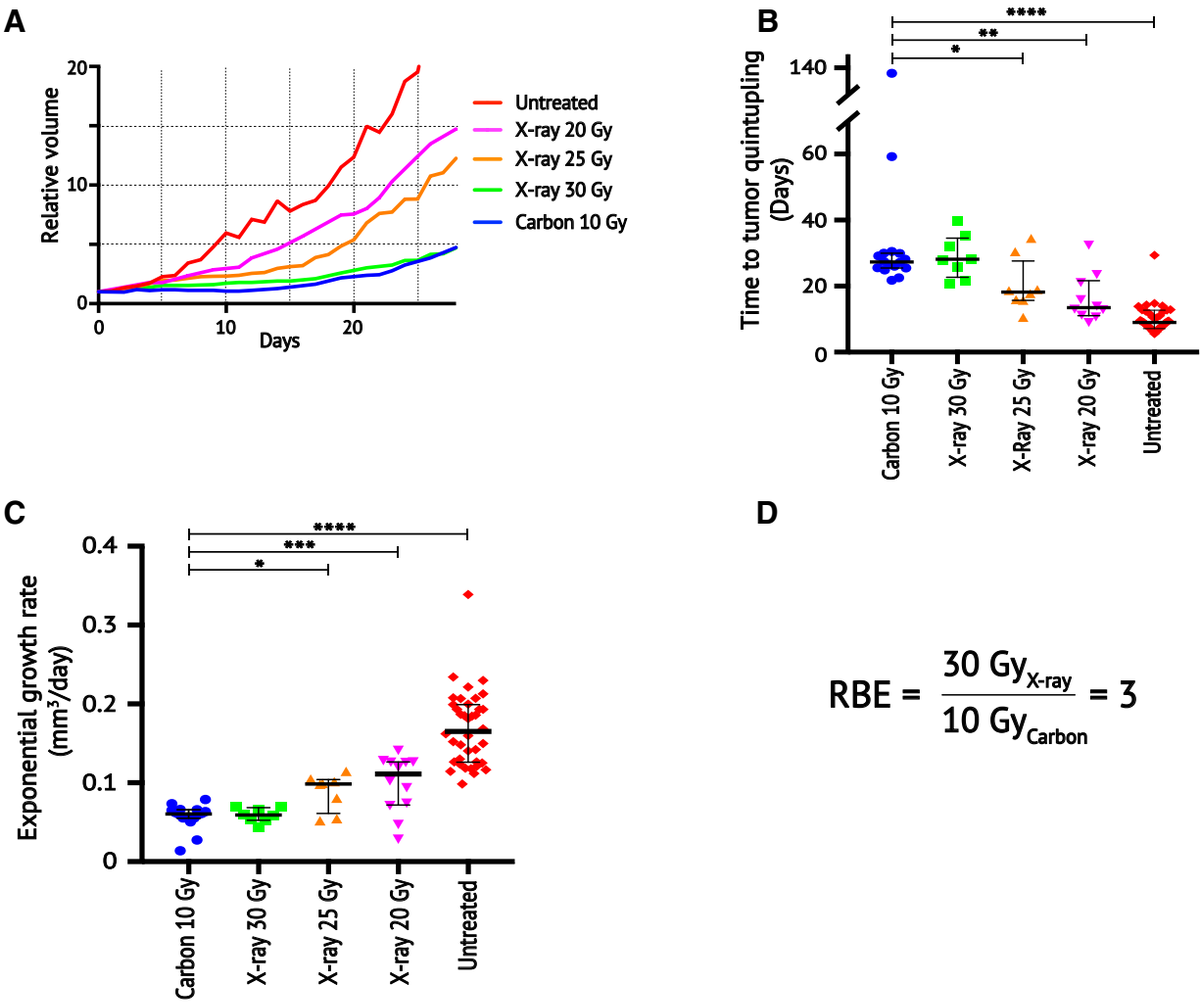

Figure 3.

Response of primary sarcomas to carbon ions and X-rays and RBE. **A,** Mean relative tumor volumes as a function of days after treatment in untreated controls (red, $n = 38$), and mice treated with single fractions of 20 Gy X-ray (purple, $n = 12$), 25 Gy X-ray (orange, $n = 8$), 30 Gy X-ray (green, $n = 8$), and 10 Gy Carbon (blue, $n = 16$). Volumes are normalized to volume on day of treatment in irradiated mice and the first measured volume >40 mm^3 for untreated controls. **B,** Data from panel (**A**) represented as number of days for tumor volume quintupling from the initial day of treatment. **C,** Data from panel (**A**) represented as the exponential growth rate for sarcomas in each treatment group. **D,** RBE is defined as the dose of X-rays divided by the dose of particle radiation required to produce the same biological result. Because 30 Gy X-rays and 10 Gy carbon ions have similar time to tumor quintupling and exponential growth rates, the RBE of carbon ions for these endpoints in primary sarcomas is 3. Median values (thick black lines) and interquartile range (IQR; thin black error bars) shown; statistical significance evaluated with Mann–Whitney *U* test. *, $P < 0.05$; **, $P < 0.01$; ***, $P < 0.001$; ****, $P < 0.0001$.

sarcomas treated with 30 Gy X-rays ($P = 0.33$). However, once tumors recurred, those treated with 10 Gy carbon enlarged more rapidly with a significantly higher exponential growth rate compared to 30 Gy X-rays, median 0.11 mm^3/day vs. 0.08 mm^3/day, respectively ($P < 0.01$).

Proliferation and stromal response

Mice were sacrificed when tumor size approached 2,000 mm^3 or when they appeared moribund. Using samples harvested at this defined endpoint, we performed Ki-67 staining on tumors treated with 10 Gy carbon, 30 Gy X-rays, and untreated controls (Fig. 5A). X-ray treated tumors had significantly fewer Ki-67 positive cells than either carbon treated tumors ($P < 0.01$) or untreated controls ($P < 0.01$; Fig. 5B). No difference in proliferation, as measured by Ki-67 staining, was detected between the carbon treated and the untreated controls. Phospho-histone H3 staining at tumor endpoint (Fig. 5C and D) similarly revealed a higher mitotic fraction in tumors treated with 10 Gy carbon compared to 30 Gy X-rays ($P < 0.01$). Furthermore, carbon treated tumors had a significantly higher mitotic index than untreated tumors ($P < 0.05$) (Fig. 5D). In contrast to the increased proliferation and mitotic fraction in carbon ion treated tumors at study endpoint, histologic examination 24 to 48 hours after treatment showed significantly less staining with phospho-histone H3 in tumors treated with 10 Gy carbon compared to 30 Gy X-rays. We observed a similar trend with Ki-67 staining, but differences did not reach statistical

Published OnlineFirst February 7, 2018; DOI: 10.1158/1535-7163.MCT-17-0965

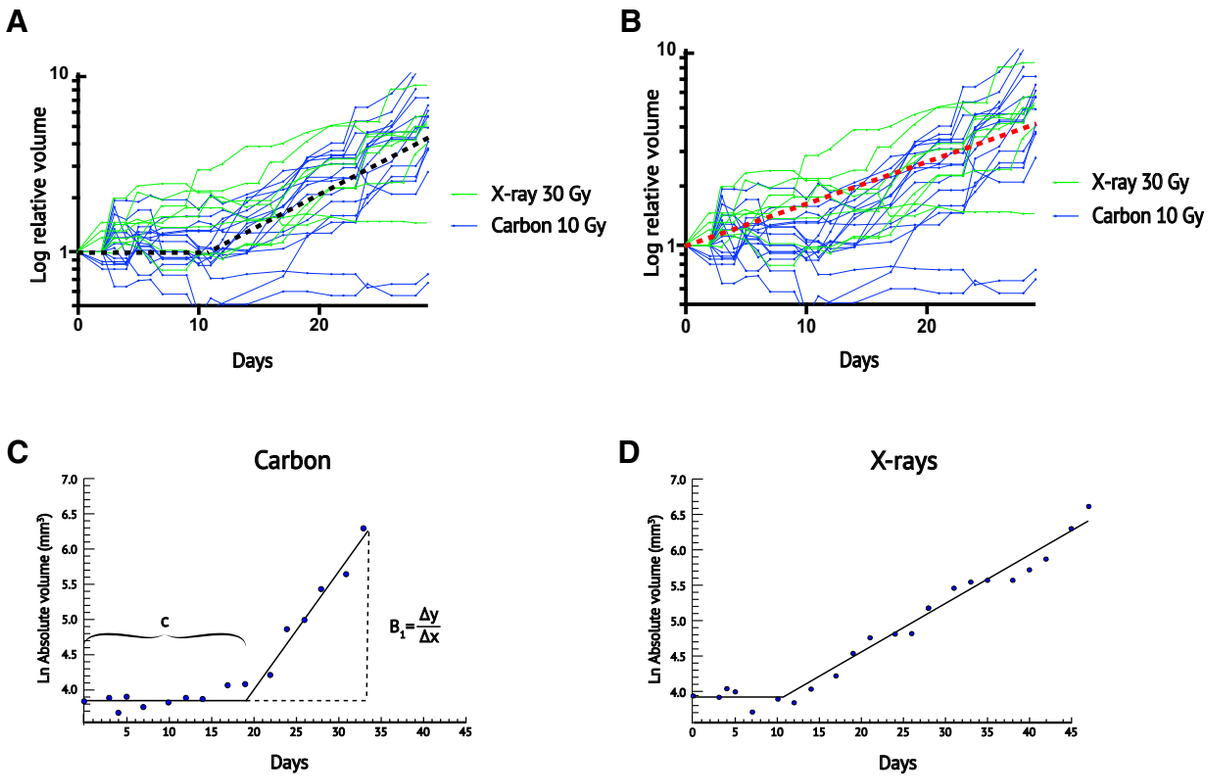

Figure 4.

Comparison of relative growth after 10 Gy carbon ions and 30 Gy X-rays using piecewise exponential and simple exponential regression models. **A,** Log relative volume as a function of time following treatment for individual tumors after 10 Gy carbon (blue) or 30 Gy X-rays (green) with a graphical representation of a piecewise exponential model (black dashed line). **B,** Volume data described in (**A**) with a graphical representation of a simple exponential model (red dashed lined)**.** Note that the piecewise model characterizes the period of post-treatment stasis and the rate of regrowth better than the simple exponential model. **C,** Example of an individual sarcoma evaluated with the piecewise exponential model after 10 Gy carbon ion radiation therapy. **D,** Example of an individual sarcoma evaluated with the piecewise exponential model after 30 Gy X-rays radiation therapy. For details of the piecewise exponential model, please refer to Eq. 2.

significance (Fig. 5E and F; Supplementary Fig. S2). Therefore, 10 Gy CIT initially caused tumor cells to divide more slowly than 30 Gy X-rays; however, as tumors began to regrow, proliferation in carbon-treated tumors accelerated, and outpaced X-ray treated tumors at the study endpoint. These findings are concordant with tumor growth modeling, which similarly showed faster growth in carbon treated sarcomas as tumors became large (Fig. 4).

Because CIT may improve activation of the immune system following treatment (12), we also stained tumors for CD3 to quantify tumor-associated T-cells. Remarkably, 24 to 48 hours after radiation, sarcomas treated with carbon ions had increased numbers of CD3+ T cells compared to sarcomas treated with isoeffective X-rays (Fig. 5G and H). However, TUNEL staining at 24 to 48 hours was similar between treatment groups (Supplementary Fig. S3). Thus, although isoeffective treatments resulted in similar tumor cell death at 1 to 2 days, their effect on the tumor stroma at this time differed with CIT eliciting larger T-cell infiltrate.

Discussion

Much of our understanding regarding how high LET radiation impacts tumor growth *in vivo* is based on xenograft (24, 25, 27, 28) and syngeneic allograft animal models (20, 26, 29). Although these transplant models are helpful tools that facilitate investigating the treatment response of cancers with a wide range of oncogenic mutations, they do not recapitulate a native tumor–stromal interaction. Primary tumor models differ from transplant models in this regard. Rather than cancer cells being implanted, the neoplastic transformation is induced in a physiologically relevant orthotopic location, allowing the tumor to coevolve with the host's intact immune system, much like human cancer (37). To our knowledge, the response of cancers to high LET radiation has never before been studied in a primary tumor model. We sought to address this critical need by characterizing the effects of CIT in a clinically relevant autochthonous mouse model of soft tissue sarcoma.

With access to the accelerator complex at BNL and an on-site animal research facility, the NASA Space Radiation Laboratory (NSRL) is currently the only U.S. center capable of heavy ion research on animals. The primary focus of NSRL is to model the health risks faced by astronauts during space travel due to high-energy particle exposure (38–40). Although the NSRL had not previously used high LET radiation with a SOBP to treat tumors *in vivo*, Held and colleagues recently advocated for this application (41). With minimal institutional precedent, the on-site particle

Published OnlineFirst February 7, 2018; DOI: 10.1158/1535-7163.MCT-17-0965

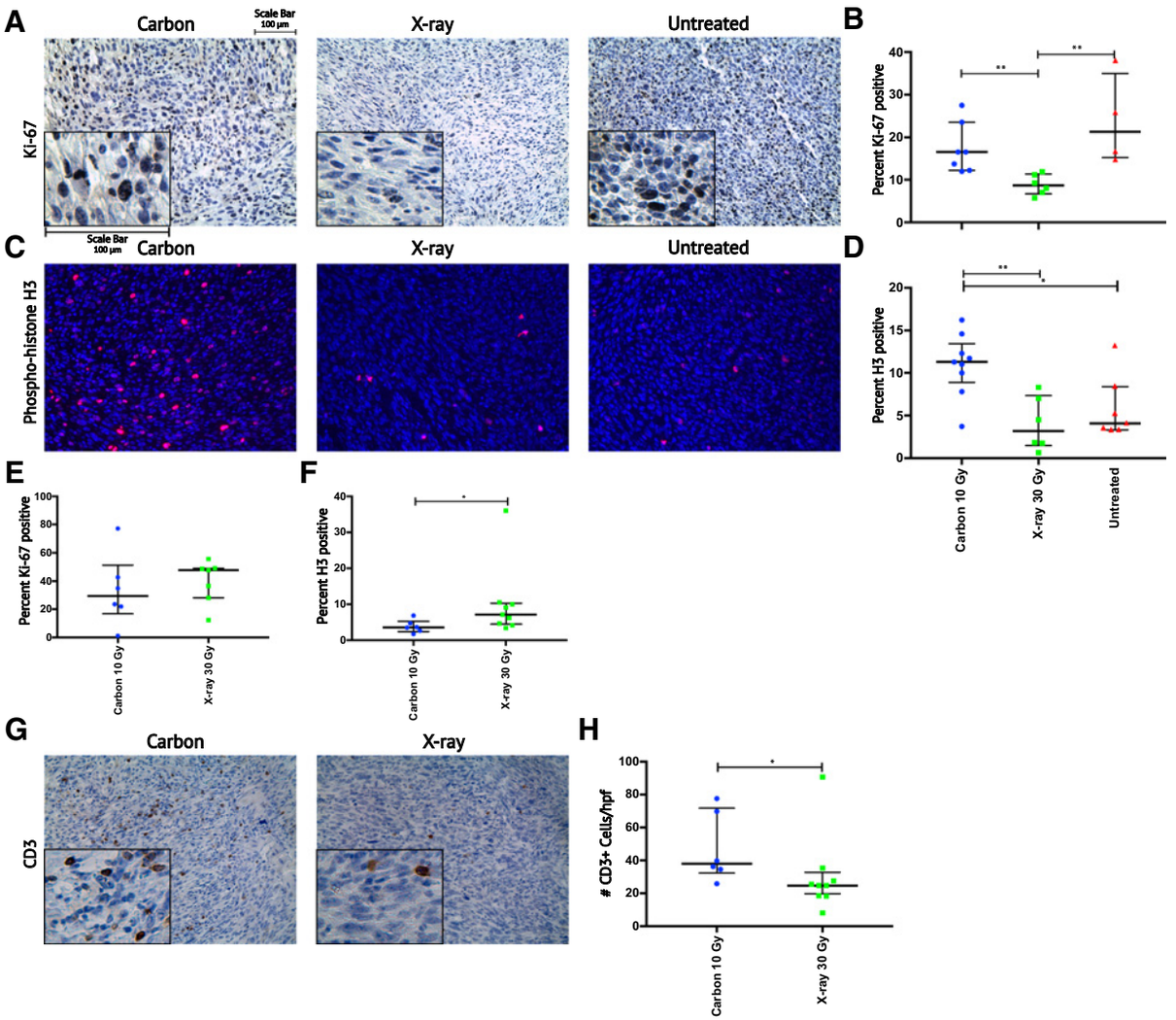

Figure 5.

Assessment of tumor cell proliferation and T-cell infiltration after carbon ion or X-ray radiotherapy. **A,** Evaluation of proliferation by Ki-67 immunohistochemistry in sarcomas treated with 10 Gy carbon ions, 30 Gy X-rays, and untreated sarcomas when tumor volume approached the limit of the IACUC protocol. **B,** Quantification of Ki-67 staining for sarcomas that reached the experimental endpoint in each treatment group. **C,** Evaluation tumor cells in G2 and mitosis by immunofluorescence of phospho-histone H3 in sarcomas treated with 10 Gy carbon ions, 30 Gy X-rays, and untreated sarcomas when tumor volume approached the limit of the IACUC protocol. **D,** Quantification of phospho-histone H3 staining for sarcomas that reached the experimental endpoint in each treatment group. **E,** Quantification of Ki-67 staining for sarcomas at 24 or 48 hours after 10 Gy carbon ions and 30 Gy X-rays$^{\Delta}$. **F,** Quantification of phospho-histone H3 staining for sarcomas at 24 or 48 hours after 10 Gy carbon ions and 30 Gy X-rays$^{\Delta}$. **G,** Evaluation of T-cell infiltration in sarcomas proliferation by CD3 immunohistochemistry at 24 or 48 hours after 10 Gy carbon ions and 30 Gy X-rays. **H,** Quantification of infiltrating T cells in sarcomas at 24 or 48 hours after 10 Gy carbon ions and 30 Gy X-rays$^{\Delta}$. Median values (thick black lines) and IQR (thin black error bars) shown; statistical significance evaluated with Mann–Whitney *U* test. *, $P < 0.05$; **, $P < 0.01$. Δ refer to Supplementary Fig. S2 for breakdown of 24 and 48 hours. Scale bar = 100 μm.

physics team successfully optimized a mono-energetic carbon ion beam for therapeutic use and built a custom device for immobilization to facilitate treatment. Indeed, ion chamber measurements and Monte Carlo simulations confirmed a homogenous 3 cm SOBP with clinically relevant LET deposited throughout the target. These results demonstrate that US researchers need not travel oversees to study hadron therapy in animal tumor models.

A crucial part of planning for our experiment was to ensure that the LET was clinically relevant. Like other charged particles, the LET of carbon ions is highest at the end of range within their Bragg peak (17, 26). The RBE is unity at 13 keV/μm (42) and increases with increasing LET, peaking at approximately 100 keV/μm (17, 18). Tumors in this experiment were treated with an LET between 57 to 61 keV/μm, which is comparable to the range used in clinical treatment centers utilizing CIT (36).

The relationship between RBE of carbon ions and fraction size is complex and depends on how fractionation changes the effectiveness of cell killing by X-rays. X-rays delivered in a single large fraction exert more damage than if the same dose is divided into multiple fractions (43). The effects of high LET radiation on cell

Published OnlineFirst February 7, 2018; DOI: 10.1158/1535-7163.MCT-17-0965

killing are less dependent on fractionation. Thus, the RBE for carbon ions decreases with increasing fraction size (19). Suzuki and colleagues treated cell lines with CIT and X-rays, and noted an RBE of 2 to 3.01 at carbon ion fractional doses of 1.4 to 3.86 Gy (15) with others reporting similar results (17). However, in studies where carbon was prescribed in larger doses per fraction like those we employed here, the RBE is lower, ranging between 1.5 and 2.7 (16, 20, 26, 29, 44). For example, Koike and colleagues treated a radioresistant murine fibrosarcoma with CIT and calculated RBE with a growth delay endpoint. With an LET of 77 keV/μm, the RBE decreased from 2.9 to 2.7 as fraction size increased from 6 to 14 Gy; and at an LET of 44 keV/μm the RBE was considerably lower, decreasing from 2.2 to 2.1 with the same doses (16). We delivered 10 Gy of CIT to primary sarcomas in mice with a median LET of 59 keV/μm and calculated an RBE of 3, which was higher than anticipated.

The relatively high potency of CIT we observed here may be multifactorial, relating to both the aggressive nature of this primary sarcoma model and host–tumor interactions. Because the destructive impacts of carbon ions are less affected by intrinsic tumor radioresistance (45) and less dependent on the presence of oxygen (18), the RBE for CIT may be increased in poorly differentiated, poorly perfused tumors where X-rays may have less efficacy. In a study comparing syngeneic mouse models of prostate cancer, Glowa and colleagues noted a significantly higher RBE in an anaplastic cell line that formed necrotic tumors as compared with a lower grade cell line (20). As the sarcomas that we studied are rapidly growing and radioresistant tumors with regions of dysfunctional vasculature and hypoxia (46), CIT may be relatively more effective than X-rays in these high-grade neoplasms.

Antitumor immunity may have also contributed to the improved relative efficacy of CIT in this primary model. We observed a more pronounced T-cell infiltrate at early time points in tumors treated with 10 Gy carbon as compared to those treated with isoeffective 30 Gy X-rays. Although there are limited data regarding how CIT affects host-tumor immunity or what role the immune system plays in tumor response to CIT, the available preclinical models suggest that CIT may better synergize with the immune system to fight cancer (47). In a murine squamous cell carcinoma transplant model, Ando and colleagues noted that injected activated dendritic cells (ADC) combined with CIT suppressed pulmonary metastases more effectively than ADCs combined with an isoeffective photon treatment (12). Our results showing increased T-cell infiltration following carbon ions compared to an isoeffective dose of X-rays is consistent with the notion that CIT may preferentially activate the immune system. Recently, two groups reported that micronuclei, which form after irradiated cells proceed through mitosis with damaged DNA, stimulate the innate immune system via interferon-stimulated gene expression (48, 49). Therefore, it is possible that CIT increases the number of micronuclei that form following radiation, which preferentially activate the immune system. In the future, it will be important to test this hypothesis using primary tumor models where a tumor co-evolves with the immune system, as well as the clinically important question of whether CIT synergizes with immunotherapy (e.g., immune checkpoint blockade) to a greater extent than X-ray therapy.

Untreated sarcomas in this mouse model grow exponentially with a constant growth rate until they reach a large volume. However, irradiation causes an initial period of stasis before exponential growth resumes. In carbon treated tumors, the effect appears to be more profound with a longer growth arrest compared to X-ray treated tumors, and quicker tumor expansion occurs once regrowth begins. We created a piecewise exponential model to quantify these effects and determine if there were differences in the kinetics of regrowth between the isoeffective carbon ion and X-ray treatments. Compared to tumors treated with X-rays, our piecewise exponential model demonstrated significantly faster regrowth in carbon-treated tumors. Histologic analysis of carbon-treated tumors at endpoint concordantly demonstrated a higher phospho-histone H3 mitotic index and Ki-67 index as compared to those treated with X-rays. We also observed a trend toward longer growth arrest with carbon and similarly noted a significantly lower phospho-histone H3 mitotic index at 24 to 48 hours following radiation. Given the high mitotic rate in recurrent KP tumor cells following carbon ion radiation, it is possible that adjuvant treatment with M-phase-specific cytotoxic chemotherapy may be even more efficacious with CIT than X-rays.

Successfully using CIT in the clinic depends on the ability to safely deliver the radiation to the tumor without causing unacceptable acute and late toxicity. For the same total radiation dose, late radiation effects are often more likely after high dose per fraction (hypofractionated) X-rays. Therefore, the RBE of carbon for late normal tissue toxicity is lower at high doses per fraction compared to smaller doses per fraction. The RBE for 66 keV/μm carbon ions for rat spinal cord myelopathy was 1.94 with a TD_{50} of 17.7 Gy delivered in two fractions (14), and the RBE for late skin fibrosis in another experiment was 1.5 (44). Given that as fraction size increases, the RBE decreases more in late responding tissues than in tumors, some have speculated that hypofractionation would improve therapeutic gain for CIT (50). Our results in a primary sarcoma model support the concept that hypofractionated carbon ions will provide therapeutic gain at 10 Gy if the RBE for critical structures is less than 3 and treatment can be delivered within normal tissue constraints.

Execution of this study was challenging because primary sarcoma development is stochastic, which makes the exact timing of tumor development difficult to predict (31). Our carbon ion beam-time was limited to 3 weekly sessions of 2 to 3 hours and was scheduled several months in advance. Because of costs and logistics, it was only feasible to irradiate 24 tumor-bearing mice at the NSRL, thus we calculated the RBE using a single dose of CIT with a growth delay endpoint. Evaluating the RBE with a tumor control endpoint utilizing numerous doses of CIT may yield additional important information about the effects of carbon ions in primary tumor models.

In conclusion, we evaluated carbon ion radiotherapy in a primary tumor mouse model of sarcoma. For a tumor growth delay endpoint, we calculated an RBE of 3, which was higher than expected based on *in vitro* data and *in vivo* transplant models. Although tumors irradiated with 10 Gy CIT and 30 Gy X-rays were isoeffective with respect to tumor quintupling time, there were important differences in both the tumor and stromal responses that have not been previously described. Having demonstrated the feasibility of completing preclinical experiments of CIT in a primary tumor model in the US, we have established a platform where investigators can study the effects of carbon ions on cancers to gain new mechanistic insights and test novel treatment strategies that may be exploited to improve therapeutic gain.

Disclosure of Potential Conflicts of Interest

No potential conflicts of interest were disclosed.

Authors' Contributions

Conception and design: J.M. Brownstein, Y.M. Mowery, P. Guida, C.-L. Lee, C. La Tessa, Y. Ma, D.G. Kirsch
Development of methodology: J.M. Brownstein, A.J. Wisdom, Y.M. Mowery, P. Guida, C.-L. Lee, L. Luo, Y. Ma, S.-H. Jung, M. Durante
Acquisition of data (provided animals, acquired and managed patients, provided facilities, etc.): J.M. Brownstein, A.J. Wisdom, K.D. Castle, Y.M. Mowery, P. Guida, C.-L. Lee, L. Luo, L. Da Silva Campos, Y. Ma, N. Williams
Analysis and interpretation of data (e.g., statistical analysis, biostatistics, computational analysis): J.M. Brownstein, A.J. Wisdom, F. Tommasino, C. La Tessa, E. Scifoni, J. Gao, Y. Ma, S.-H. Jung, M. Durante, D.G. Kirsch
Writing, review, and/or revision of the manuscript: J.M. Brownstein, A.J. Wisdom, K.D. Castle, Y.M. Mowery, F. Tommasino, E. Scifoni, J. Gao, L. Da Silva Campos, Y. Ma, S.-H. Jung, D.G. Kirsch
Administrative, technical, or material support (i.e., reporting or organizing data, constructing databases): J.M. Brownstein, A.J. Wisdom, J. Gao, L. Luo, L. Da Silva Campos, Y. Ma, N. Williams
Study supervision: Y. Ma, D.G. Kirsch

Acknowledgments

This work was supported by the NCI (NIH; 1R35CA197616) and the Barbara Levine University Professorship to D.G. Kirsch. We thank Tyler Jacks (MIT) for providing the *LSL-Kras*^{G12D} mice and Anton Berns (NKI) for providing the *p53*^{FL} mice. We thank Adam Rusek for facilitating carbon ion therapy at the NASA Space Radiation Laboratory.

The costs of publication of this article were defrayed in part by the payment of page charges. This article must therefore be hereby marked *advertisement* in accordance with 18 U.S.C. Section 1734 solely to indicate this fact.

Received September 29, 2017; revised December 28, 2017; accepted February 1, 2018; published first February 7, 2018.

References

1. Howlader NNA, Krapcho M, Miller D, Bishop K, Kosary CL, Yu M, et al. (eds). SEER Cancer Statistics Review, 1975–2014. National Cancer Institute. Novermber 2016 ed: Bethesda, MD; 2016.
2. Page BR, Hudson AD, Brown DW, Shulman AC, Abdel-Wahab M, Fisher BJ, et al. Cobalt, linac, or other: what is the best solution for radiation therapy in developing countries? Int J Radiat Oncol Biol Phys 2014;89:476–80.
3. Mohan R, Grosshans D. Proton therapy – present and future. Adv Drug Deliv Rev 2017;109:26–44.
4. Wang X, Krishnan S, Zhang X, Dong L, Briere T, Crane CH, et al. Proton radiotherapy for liver tumors: dosimetric advantages over photon plans. Med Dosim 2008;33:259–67.
5. Glimelius B, Isacsson U, Blomquist E, Grusell E, Jung B, Montelius A. Potential gains using high-energy protons for therapy of malignant tumours. Acta Oncol 1999;38:137–45.
6. Rombi B, Vennarini S, Vinante L, Ravanelli D, Amichetti M. Proton radiotherapy for pediatric tumors: review of first clinical results. Ital J Pediatr 2014;40:74.
7. Durante M, Loeffler JS. Charged particles in radiation oncology. Nat Rev Clin Oncol 2010;7:37–43.
8. Mohamad O, Sishc BJ, Saha J, Pompos A, Rahimi A, Story MD, et al. Carbon ion radiotherapy: a review of clinical experiences and preclinical research, with an emphasis on DNA damage/repair. Cancers (Basel) 2017;9:66.
9. Ebner DK, Kamada T. The emerging role of carbon-ion radiotherapy. Front Oncol 2016;6:140.
10. Desouky O, Zhou G. Biophysical and radiobiological aspects of heavy charged particles. J Taibah University Sci 2016;10:187–94.
11. Hirayama R, Ito A, Tomita M, Tsukada T, Yatagai F, Noguchi M, et al. Contributions of direct and indirect actions in cell killing by high-LET radiations. Radiat Res 2009;171:212–8.
12. Ando K, Fujita H, Hosoi A, Ma L, Wakatsuki M, Seino KI, et al. Intravenous dendritic cell administration enhances suppression of lung metastasis induced by carbon-ion irradiation. J Radiat Res 2017;58:446–55.
13. Ogata T, Teshima T, Kagawa K, Hishikawa Y, Takahashi Y, Kawaguchi A, et al. Particle irradiation suppresses metastatic potential of cancer cells. Cancer Res 2005;65:113–20.
14. Saager M, Glowa C, Peschke P, Brons S, Grun R, Scholz M, et al. Split dose carbon ion irradiation of the rat spinal cord: dependence of the relative biological effectiveness on dose and linear energy transfer. Radiother Oncol 2015;117:358–63.
15. Suzuki M, Kase Y, Yamaguchi H, Kanai T, Ando K. Relative biological effectiveness for cell-killing effect on various human cell lines irradiated with heavy-ion medical accelerator in Chiba (HIMAC) carbon-ion beams. Int J Radiat Oncol Biol Phys 2000;48:241–50.
16. Koike S, Ando K, Oohira C, Fukawa T, Lee R, Takai N, et al. Relative biological effectiveness of 290 MeV/u carbon ions for the growth delay of a radioresistant murine fibrosarcoma. J Radiat Res 2002;43:247–55.
17. Elsasser T, Weyrather WK, Friedrich T, Durante M, Iancu G, Kramer M, et al. Quantification of the relative biological effectiveness for ion beam radiotherapy: direct experimental comparison of proton and carbon ion beams and a novel approach for treatment planning. Int J Radiat Oncol Biol Phys 2010;78:1177–83.
18. Furusawa Y, Fukutsu K, Aoki M, Itsukaichi H, Eguchi-Kasai K, Ohara H, et al. Inactivation of aerobic and hypoxic cells from three different cell lines by accelerated (3)He-, (12)C- and (20)Ne-ion beams. Radiat Res 2000;154:485–96.
19. Friedrich T, Scholz U, Durante M, Scholz M. RBE of ion beams in hypofractionated radiotherapy (SBRT). Phys Med 2014;30:588–91.
20. Glowa C, Karger CP, Brons S, Zhao D, Mason RP, Huber PE, et al. Carbon ion radiotherapy decreases the impact of tumor heterogeneity on radiation response in experimental prostate tumors. Cancer Lett 2016;378:97–103.
21. Hammel P, Huguet F, van Laethem J-L, Goldstein D, Glimelius B, Artru P, et al. Effect of chemoradiotherapy vs. chemotherapy on survival in patients with locally advanced pancreatic cancer controlled after 4 months of gemcitabine with or without erlotinib: the LAP07 randomized clinical trial. JAMA 2016;315:1844–53.
22. Shinoto M, Yamada S, Terashima K, Yasuda S, Shioyama Y, Honda H, et al. Carbon ion radiation therapy with concurrent gemcitabine for patients with locally advanced pancreatic cancer. Int J Radiat Oncol Biol Phys 2016;95:498–504.
23. Hahnloser D, Nelson H, Gunderson LL, Hassan I, Haddock MG, O'Connell MJ, et al. Curative potential of multimodality therapy for locally recurrent rectal cancer. Ann Surg 2003;237:502–8.
24. Subtil FS, Wilhelm J, Bill V, Westholt N, Rudolph S, Fischer J, et al. Carbon ion radiotherapy of human lung cancer attenuates HIF-1 signaling and acts with considerably enhanced therapeutic efficiency. FASEB J 2014;28:1412–21.
25. Sai S, Wakai T, Vares G, Yamada S, Kamijo T, Kamada T, et al. Combination of carbon ion beam and gemcitabine causes irreparable DNA damage and death of radioresistant pancreatic cancer stem-like cells in vitro and in vivo. Oncotarget 2015;6:5517–35.
26. Peschke P, Karger CP, Scholz M, Debus J, Huber PE. Relative biological effectiveness of carbon ions for local tumor control of a radioresistant prostate carcinoma in the rat. Int J Radiat Oncol Biol Phys 2011;79:239–46.
27. Kano M, Yamada S, Hoshino I, Murakami K, Akutsu Y, Sakata H, et al. Effects of carbon-ion radiotherapy combined with a novel histone deacetylase inhibitor, cyclic hydroxamic-acid-containing peptide 31 in human esophageal squamous cell carcinoma. Anticancer Res 2009;29:4433–8.
28. Cui X, Oonishi K, Tsujii H, Yasuda T, Matsumoto Y, Furusawa Y, et al. Effects of carbon ion beam on putative colon cancer stem cells and its comparison with X-rays. Cancer Res 2011;71:3676–87.

Published OnlineFirst February 7, 2018; DOI: 10.1158/1535-7163.MCT-17-0965

29. Ando K, Koike S, Uzawa A, Takai N, Fukawa T, Furusawa Y, et al. Biological gain of carbon-ion radiotherapy for the early response of tumor growth delay and against early response of skin reaction in mice. J Radiat Res 2005;46:51–7.
30. Moding EJ, Castle KD, Perez BA, Oh P, Min HD, Norris H, et al. Tumor cells but not endothelial cells mediate the eradication of primary sarcomas by stereotactic body radiation therapy(). Sci Transl Med 2015;7:278ra34.
31. Kirsch DG, Dinulescu DM, Miller JB, Grimm J, Santiago PM, Young NP, et al. A spatially and temporally restricted mouse model of soft tissue sarcoma. Nat Med 2007;13:992–7.
32. Mito JK, Riedel RF, Dodd L, Lahat G, Lazar AJ, Dodd RD, et al. Cross species genomic analysis identifies a mouse model as undifferentiated pleomorphic sarcoma/malignant fibrous histiocytoma. PLoS One 2009;4:e8075.
33. Newton J, Oldham M, Thomas A, Li Y, Adamovics J, Kirsch DG, et al. Commissioning a small-field biological irradiator using point, 2D, and 3D dosimetry techniques. Med Phys 2011;38:6754–62.
34. Cirrone GP, Cuttone G, Mazzaglia SE, Romano F, Sardina D, Agodi C, et al. Hadrontherapy: a Geant4-based tool for proton/ion-therapy studies. Prog Nucl Sci Technol 2011;2:207–12.
35. Jia SB, Romano F, Cirrone GAP, Cuttone G, Hadizadeh MH, Mowlavi AA, et al. Designing a range modulator wheel to spread-out the Bragg peak for a passive proton therapy facility. Nucl Instrum Methods Phys Res A 2016; 806:101–8.
36. Bassler N, Jakel O, Sondergaard CS, Petersen JB. Dose- and LET-painting with particle therapy. Acta Oncol 2010;49:1170–6.
37. Castle KD, Chen M, Wisdom AJ, Kirsch DG. Genetically engineered mouse models for studying radiation biology. Transl Cancer Res 2017: S900–S13.
38. Durante M, George K, Gialanella G, Grossi G, La Tessa C, Manti L, et al. Cytogenetic effects of high-energy iron ions: dependence on shielding thickness and material. Radiat Res 2005;164:571–6.
39. Norbury JW, Schimmerling W, Slaba TC, Azzam EI, Badavi FF, Baiocco G, et al. Galactic cosmic ray simulation at the NASA Space Radiation Laboratory. Life Sci Space Res (Amst) 2016;8:38–51.
40. Schimmerling W. Genesis of the NASA Space Radiation Laboratory. Life Sci Space Res (Amst) 2016;9:2–11.
41. Held KD, Blakely EA, Story MD, Lowenstein DI. Use of the NASA Space Radiation Laboratory at Brookhaven National Laboratory to conduct charged particle radiobiology studies relevant to ion therapy. Radiat Res 2016;185:563–7.
42. Suman S, Datta K, Trani D, Laiakis EC, Strawn SJ, Fornace AJ Jr. Relative biological effectiveness of 12C and 28Si radiation in C57BL/6J mice. Radiat Environ Biophys 2012;51:303–9.
43. Hall EJ, Giaccia AJ. Radiobiology for the radiologist. Philadelphia: Wolters Kluwer Health/Lippincott Williams & Wilkins; 2012. ix, p. 546.
44. Sorensen BS, Horsman MR, Alsner J, Overgaard J, Durante M, Scholz M, et al. Relative biological effectiveness of carbon ions for tumor control, acute skin damage and late radiation-induced fibrosis in a mouse model. Acta Oncol 2015;54:1623–30.
45. Broerse JJ, Barendsen GW. Relative biological effectiveness of fast neutrons for effects on normal tissues. Curr Top Radiat Res Q 1973;8:305–50.
46. Moding EJ, Clark DP, Qi Y, Li Y, Ma Y, Ghaghada K, et al. Dual-energy micro-computed tomography imaging of radiation-induced vascular changes in primary mouse sarcomas. Int J Radiat Oncol Biol Phys 2013;85:1353–9.
47. Durante M, Brenner DJ, Formenti SC. Does heavy ion therapy work through the immune system? Int J Radiat Oncol Biol Phys 2016;96:934–6.
48. Harding SM, Benci JL, Irianto J, Discher DE, Minn AJ, Greenberg RA. Mitotic progression following DNA damage enables pattern recognition within micronuclei. Nature 2017;548:466–70.
49. Mackenzie KJ, Carroll P, Martin CA, Murina O, Fluteau A, Simpson DJ, et al. cGAS surveillance of micronuclei links genome instability to innate immunity. Nature 2017;548:461–5.
50. Schulz-Ertner D, Tsujii H. Particle radiation therapy using proton and heavier ion beams. J Clin Oncol 2007;25:953–64.

Published OnlineFirst February 7, 2018; DOI: 10.1158/1535-7163.MCT-17-0965

Molecular Cancer Therapeutics

Characterizing the Potency and Impact of Carbon Ion Therapy in a Primary Mouse Model of Soft Tissue Sarcoma

Jeremy M. Brownstein, Amy J. Wisdom, Katherine D. Castle, et al.

Mol Cancer Ther 2018;17:858-868. Published OnlineFirst February 7, 2018.